PHYSICAL REVIEW B VOLUME 36, NUMBER 8 15 SEPTEMBER 1987-I

Γ-X mixing in GaAs/$Al_xGa_{1-x}As$ and $Al_xGa_{1-x}As$/AlAs superlattices

D. Z. -Y. Ting and Yia-Chung Chang
Department of Physics and Materials Research Laboratory, University of Illinois at Urbana-Champaign, Urbana, Illinois 61801

(Received 6 February 1987; revised manuscript received 11 May 1987)

A systematic study of the conduction bands of the (001) GaAs/$Al_xGa_{1-x}As$ and $Al_xGa_{1-x}As$/AlAs superlattices using a one-band Wannier orbital model is presented. The parameters in the Wannier orbital model are fitted to correctly describe the lowest conduction band of the bulk semiconductors over the entire Brillouin zone, including the correct effective masses. Using this model, we have examined the dependence of the superlattice conduction-band energy levels on layer thicknesses, alloy composition, and wave vectors, as well as external hydrostatic pressure. We have found that there can be substantial mixing between the Γ-valley states and the (001) X-valley states. The symmetry of the confined X-valley states is found to be critically dependent on whether the slabs with higher Al concentration contain an even or odd number of monolayers. As a result, the amount of Γ-X mixing is extremely sensitive to the layer thicknesses. An experimental procedure for observing this effect with use of high-quality samples of superlattices with ultrathin layers is proposed. Our calculations also show that the pressure coefficients associated with the Γ-like quantum-well states decrease with well width; the results are in good agreement with experimental data. In addition, mixing between states derived from the (100) and (010) X valleys is also reported.

I. INTRODUCTION

In 1970 Esaki and Tsu[1] first proposed fabricating superlattices from alternating layers of semiconducting materials. Since then a variety of superlattices have been grown.[2,3] Because of their technological importance, superlattices have been widely investigated both experimentally and theoretically. The theory of superlattice valence bands has recently been extensively studied by a number of groups.[4–6] The conduction bands of superlattices can be treated adequately by the Kronig-Penney model, provided that the superlattices are made from a direct-band-gap semiconductor where only the Γ-valley electrons need to be considered. Recently, however, there has been considerable interest in systems such as the $GaAs_{1-x}P_x$/GaP (Refs. 7 and 8) and the GeSi/Si (Ref. 9) strained-layer superlattices (SLS) and the $Al_xGa_{1-x}As$/AlAs superlattice which are made from indirect-band-gap semiconductors. For these systems we must take into account electrons associated with the various conduction-band valleys (Γ, X, L, etc.). Moreover, even for a GaAs/$Al_xGa_{1-x}As$ superlattice which is made entirely from direct-band-gap semiconductors, external hydrostatic pressure can be applied to drive the Γ-valley states up in energy so that the X-valley states become the lowest conduction-band states.

Recently, several experiments have been performed to determine the band offset in $Al_xGa_{1-x}As$ heterostructures by probing the X-valley states in the GaAs/$Al_xGa_{1-x}As$ (Refs. 10 and 11) and $Al_xGa_{1-x}As$/AlAs (Ref. 12) heterostructures. Strong optical transitions between the $Ga_{1-x}As_xP$/GaP superlattice valence-band states and the X-valley states have been observed.[8] Excitons associated with the X-valley states in the ultrathin GaAs-AlAs superlattices have recently been seen.[13] To understand these experimental data, detailed knowledge of the X-valley states in superlattices is needed. In order to investigate the properties of these superlattices theoretically, realistic band structures with correct effective masses for both Γ and X valleys must be included. Previously, Jaros and co-workers studied the GeSi/Si SLS (Ref. 14) and the GaAs/$Al_xGa_{1-x}As$ (Ref. 15) superlattice with the pseudopotential method which uses a plane-wave basis; Ting and Chang also investigated the GeSi/Si SLS with a two-band model[16] which employs a localized basis with two basis orbitals per unit cell. In this paper we present another method which uses a localized basis for treating the conduction bands of superlattices. This model is simpler and numerically more efficient than the two-band model.[16] In our model the superlattice conduction-band states are constructed from the Wannier orbitals associated with the lowest conduction band of the constituent bulk semiconductors. The advantages of this approach can best be illustrated by comparing it with another method which uses a localized orbital basis, namely, the nearest-neighbor tight-binding (NNTB) model. For III-V compound semiconductors, typically eight or ten orbitals per unit cell are used in the NNTB model, while only one orbital per unit cell is needed in our model. This accounts for the computational efficiency of our model. In addition, while our model incorporates the correct effective masses for the various conduction-band valleys, the NNTB model suffers from having an infinite transverse X-valley effective mass, leading inevitably to the wrong conclusions on the superlattice X-valley states. It should be noted that the pseudopotential method also has difficulty in getting accurate effective masses. We point out that the present one-band model yields information only on the superlattice conduction bands. The valence bands must be obtained separately by other methods.[4–6] Additionally, the one-band Wannier orbital model implicitly assumes that the superlattice conduction bands of interest (i.e., the lowest few bands) have contributions only from the lowest conduction band of the bulk semiconductors. Therefore it is not suitable as the two-band model[16] is, for the treatment of superlattices such as the GeSi/Si SLS where the lowest two conduction bands are degenerate at the X point and contributions from both bands must be taken into account. Note that this is not a problem for the $\mathrm{Al}_x\mathrm{Ga}_{1-x}\mathrm{As}$ systems under consideration in this paper.

By exploiting the computational efficiency of the one-band Wannier orbital model, we have been able to examine the conduction bands of the (001) GaAs/$\mathrm{Al}_x\mathrm{Ga}_{1-x}\mathrm{As}$ and $\mathrm{Al}_x\mathrm{Ga}_{1-x}\mathrm{As}$/AlAs superlattices under a wide variety of circumstances. Specifically, we have studied the dependence of the superlattice conduction bands on layer thicknesses, alloy composition, wave vectors, and hydrostatic pressure. The remainder of this paper is organized as follows. In Sec. II we describe the one-band model and how it is implemented to treat superlattices. In Sec. III we present our results on the (001) GaAs/$\mathrm{Al}_x\mathrm{Ga}_{1-x}\mathrm{As}$ and $\mathrm{Al}_x\mathrm{Ga}_{1-x}\mathrm{As}$/AlAs superlattices. The summary is given in Sec. IV.

II. THEORY

In this section we present a theoretical method for studying the conduction bands of superlattices whose well and barrier materials can be either direct- or indirect-band-gap semiconductors. In this method the superlattice conduction bands are constructed from the lowest conduction bands of the bulk well and barrier materials; the valence bands and the higher conduction bands are discarded to achieve numerical efficiency. Thus, for instance, only the fifth band of $\mathrm{Al}_x\mathrm{Ga}_{1-x}\mathrm{As}$ and the fifth band of AlAs are used to construct the conduction bands of the $\mathrm{Al}_x\mathrm{Ga}_{1-x}\mathrm{As}$/AlAs superlattice.

A. One-band Wannier orbital model

We use the one-band Wannier orbital model to describe the lowest conduction band of bulk semiconductors. Let $|\mathbf{k}\rangle$ be the lowest bulk conduction-band state with energy $E(\mathbf{k})$. The Wannier orbital located at the lattice vector $\mathbf{R}$ is defined as

$$|\mathbf{R}\rangle=\frac{1}{\sqrt{N}}\sum_{\mathbf{k}}\exp(-i\mathbf{k}\cdot\mathbf{R})|\mathbf{k}\rangle\ , \qquad (1)$$

where N is the number of primitive cells in the bulk. The conduction-band energy $E(\mathbf{k})$ is related to the Wannier orbitals as follows:

$$E(\mathbf{k})=\langle\mathbf{k}|H|\mathbf{k}\rangle=\sum_{\mathbf{R}}\exp(i\mathbf{k}\cdot\mathbf{R})\langle\mathbf{O}|H|\mathbf{R}\rangle\ , \qquad (2)$$

where $\langle\mathbf{O}|$ denotes a Wannier orbital located at the origin.

Note that in the above expression we sum over an infinite number of Wannier orbital matrix elements $\langle\mathbf{O}|H|\mathbf{R}\rangle$ to obtain the energy $E(\mathbf{k})$. In practice we impose a cutoff on the range of interaction and only retain those terms with $|\mathbf{R}|^2\le R_C^2$, where R_C^2 is a chosen cutoff value. The set of $\langle\mathbf{O}|H|\mathbf{R}\rangle$'s are treated as adjustable parameters, and are obtained by fitting the band structure. For convenience, we shall call these fitted matrix elements one-band parameters. Two sets of one-band parameters must be fitted, one each for the well and barrier materials. Proper band offsets are added to the on-site elements ($\langle\mathbf{O}|H|\mathbf{O}\rangle$) of the two materials to ensure the correct band lineup in a superlattice. The effect of external hydrostatic pressure on the band structure is included by properly modifying the one-band parameters. A more-detailed discussion on the one-band Wannier orbital model is given in the Appendix.

Figure 1 shows the lowest conduction band of GaAs. The open squares represent the values obtained by the pseudopotential method, but slightly adjusted so that the effective masses and positions of the symmetry points agree better with experimental values. The solid curve is the one-band Wannier orbital model band structure which we fitted. As we can see, the one-band model can give us a good description of the lowest conduction band over the entire Brillouin zone.

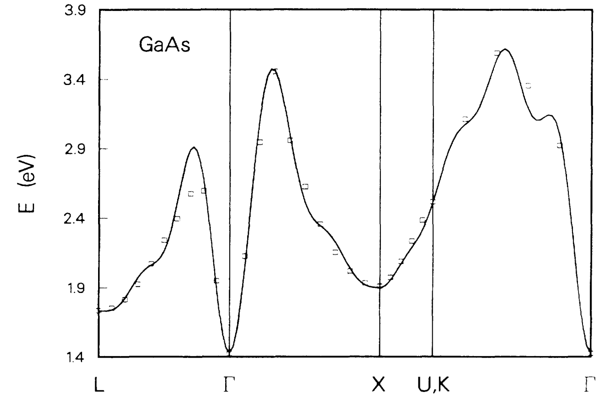

FIG. 1. Lowest conduction band of GaAs. The open squares represent the values obtained by the pseudopotential method, but slightly adjusted so that the effective masses and positions of the symmetry points agree better with experimental values. The solid curve is the one-band Wannier orbital model band structure which we fitted.

B. Implementation of the slab method

In this section we describe how we compute superlattice conduction bands using the one-band Wannier orbital model and the "slab method." The slab method is a standard method for obtaining the band structure of superlattices. We will discuss how this method is implemented for our one-band Wannier orbital model. Specifically we will be considering superlattices made from semiconductors with diamond and zinc-blende structures, and in particular we will be studying superlattices whose interface planes are perpendicular to the normal vectors $\hat{\mathbf{n}}=(0,0,1)$ and $\hat{\mathbf{n}}=(1,1,1)/\sqrt{3}$. The (0,0,1) and (1,1,1) superlattices are the most commonly grown superlattices. A feature shared by the (0,0,1) and (1,1,1) superlattices is that they both consist of alternating cation and anion atomic planes perpendicular to the growth axis. We refer to a pair of adjacent cation and anion planes as a "monolayer," or simply a "layer." A period of the superlattice will be referred to as a "superlayer." We assume that each superlayer of the superlattice under consideration consists of L_W layers of well material and L_B layers of barrier material. Our designation of well and barrier materials is determined by the valence band, i.e., the material with the higher valence-band top is designated as the well material. Note that the material with the lower conduction bottom could either be the well material or the barrier material. We will discuss this more when we present our results on the GaAs/Al$_x$Ga$_{1-x}$As and Al$_x$Ga$_{1-x}$As/AlAs superlattices.

We proceed to describe how we implement the slab method for the one-band Wannier orbital model. We begin by changing our notation of the Wannier orbitals to make it more suitable for the treatment of superlattices. In our current notation we refer to the Wannier orbitals by their Cartesian coordinates. In a superlattice, it is more convenient to refer to the Wannier orbitals by the planes they belong to, and by their positions within a given plane. Thus we define the following:

$$|\mathbf{R}_{\parallel}\sigma\rangle \equiv |\mathbf{R}\rangle \ .$$

In the above equation the unit cell label $\mathbf{R}$ is now broken into components parallel and perpendicular to the superlattice interfaces

$$\mathbf{R}=\mathbf{R}_{\parallel}+\mathbf{R}_{\perp} \ ,$$

with the perpendicular component rewritten as

$$\mathbf{R}_{\perp}=(\mathbf{R}\cdot\hat{\mathbf{n}})\hat{\mathbf{n}}=\sigma d\hat{\mathbf{n}}=\sigma\mathbf{d} \ ,$$

where σ is an integer used to label the monolayers, and d is the distance between two adjacent monolayers.

We now define the planar orbitals. In a superlattice the perpendicular component of the crystal momentum $\mathbf{k}$ is no longer a good quantum number. However, since translational invariance is still valid in the directions parallel to the interface planes, $\mathbf{k}_{\parallel}$ is still a good quantum number. Accordingly we could define planar orbitals by taking the Bloch sum of all Wannier orbitals within a given atomic plane parallel to the interfaces:

$$|\sigma,\mathbf{k}_{\parallel}\rangle=\frac{1}{(N_{\parallel})^{1/2}}\sum_{\mathbf{R}_{\parallel}}\exp(i\mathbf{k}_{\parallel}\cdot\mathbf{R}_{\parallel})\,|\mathbf{R}_{\parallel}\sigma\rangle \ , \tag{3}$$

where $N_{\parallel}$ is the number of unit cells in a layer.

The superlattice basis is formed by taking a Bloch sum of all planar orbitals which have the same relative position within the superlayer they belong to:

$$|\lambda;\mathbf{k}_{\parallel}\mathbf{q}\rangle=\frac{1}{(N_P)^{1/2}}\sum_{S}\exp(iSL\,\mathbf{q}\cdot\mathbf{d})\,|SL+\lambda;\mathbf{k}_{\parallel}\rangle \ , \tag{4}$$

$$\lambda=1,2,\ldots,L \ . \tag{5}$$

In the above expression N_P is the total number of superlayers or periods in the superlattice, $L=L_W+L_B$ is the number of layers in a superlayer, S is an integer used to label the superlayers, λ specifies the position of a layer within a superlayer, and $\mathbf{q}=q\hat{\mathbf{n}}$ is the perpendicular component of the wave vector in the mini-Brillouin-zone. Note that q takes on values between $-(\pi/Ld)$ and (π/Ld). For the well material, $1\le\lambda\le L_W$; and for the barrier material, $L_W+1\le\lambda\le L_W+L_B$. Note that for a fixed wave vector $\mathbf{k}_{\parallel}+\mathbf{q}$ there is a set of L such basis vectors corresponding to the L layers. Since the superlattice Hamiltonian is diagonal in $\mathbf{k}_{\parallel}+\mathbf{q}$, the band structure is obtained by diagonalizing the Hamiltonian within this basis set.

To obtain the matrix elements of the superlattice Hamiltonian, we start out by writing the matrix elements between the superlattice basis vectors in terms of matrix elements between planar orbitals:

$$\langle\lambda;\mathbf{k}_{\parallel}\mathbf{q}\,|\,H\,|\,\lambda';\mathbf{k}_{\parallel}\mathbf{q}\rangle =\sum_{S}\exp(-iSL\,\mathbf{q}\cdot\mathbf{d})\langle SL+\lambda;\mathbf{k}_{\parallel}\,|\,H\,|\,\lambda';\mathbf{k}_{\parallel}\rangle \ . \tag{6}$$

Note that if the separation between the two planes involved exceeds the cutoff interaction range of the one-band Wannier model, then the matrix element is 0. In fact, if we choose L_Wd and L_Bd to be greater than the cutoff interaction range (typically a few layers), then only one term in the above summation could be nonzero:

$$\langle\lambda;\mathbf{k}_{\parallel}\mathbf{q}\,|\,H\,|\,\lambda';\mathbf{k}_{\parallel}\mathbf{q}\rangle =\exp(-iS_0L\,\mathbf{q}\cdot\mathbf{d})\langle S_0L+\lambda;\mathbf{k}_{\parallel}\,|\,H\,|\,\lambda';\mathbf{k}_{\parallel}\rangle \ , \tag{7}$$

where S_0 is -1, 0, or 1, whichever minimizes the separation between the two planes at $S_0L+\lambda$ and λ'.

The matrix elements between planar orbitals can in turn be written in terms of the matrix elements between the Wannier orbitals as follows:

$$\langle\sigma;\mathbf{k}_{\parallel}\,|\,H\,|\,\sigma';\mathbf{k}_{\parallel}\rangle=\sum_{\mathbf{R}_{\parallel}}\exp(-i\mathbf{k}_{\parallel}\cdot\mathbf{R})\langle\mathbf{R}_{\parallel}\sigma\,|\,H\,|\,\mathbf{O}_{\parallel}\sigma'\rangle \ . \tag{8}$$

In the above equation we have used the fact that $\mathbf{k}_{\parallel}\cdot\mathbf{R}_{\perp}=0$ to make the exponential phase factors dependent on the lattice coordinates rather than their parallel components; this is done to make computation more efficient. Note that some of the terms in the above equation involve interactions between Wannier orbitals belonging to different materials. In such cases we take the interaction to be the average between those of the two materials.

To summarize what has been done thus far: We have constructed a superlattice basis set out of the one-band Wannier model basis orbitals, and then reduced the superlattice Hamiltonian matrix elements in terms of the one-band parameters which we know from the preceding section. We are now able to compute the matrix elements of the superlattice Hamiltonian. Diagonalizing this matrix yields the conduction-band structure of the superlattice.

C. Superlattice envelope functions

The superlattice Hamiltonian can be diagonalized to yield the superlattice energy and eigenstates:

$$H \mid n,\mathbf{k}_{\parallel}\mathbf{q}\rangle = E_n(\mathbf{k}_{\parallel}\mathbf{q}) \mid n,\mathbf{k}_{\parallel}\mathbf{q}\rangle \ , \tag{9}$$

$$\mid n,\mathbf{k}_{\parallel}\mathbf{q}\rangle = \sum_{\lambda} C^n_{\lambda}(\mathbf{k}_{\parallel}\mathbf{q}) \mid \lambda;\mathbf{k}_{\parallel}\mathbf{q}\rangle \ . \tag{10}$$

In the above equation $C^n_{\lambda}(\mathbf{k}_{\parallel}\mathbf{q})$ is the envelope function in coordinate space. By plotting $C^n_{\lambda}(\mathbf{k}_{\parallel}\mathbf{q})$ against λ, the layer label, we can find out how the superlattice wave function is distributed in space. It is often more useful, however, to examine the envelope functions in k space. this can be done by taking the equation above through a series of linear transformations and writing down the superlattice eigenfunctions in terms of the eigenfunctions of the bulk well and barrier materials. The derivation is straightforward but rather tedious. We will just write down the results:

$$\mid n,\mathbf{k}_{\parallel}\mathbf{q}\rangle = \sum_{l=1}^{L} [\, F_n(\mathbf{k}_{\parallel}\mathbf{q},\mathbf{g}_l;W) \mid \mathbf{k}_{\parallel}(\mathbf{q}+\mathbf{g}_l);W\rangle + F_n(\mathbf{k}_{\parallel}\mathbf{q},\mathbf{g}_l;B) \mid \mathbf{k}_{\parallel}(\mathbf{q}+\mathbf{g}_l);B\rangle \,] \ , \tag{11}$$

where $F_n(\mathbf{k}_{\parallel}\mathbf{q},\mathbf{g}_l;W)$ and $F_n(\mathbf{k}_{\parallel}\mathbf{q},\mathbf{g}_l;B)$ are, respectively, envelope functions in k space for the well and barrier materials. Note that in our notation for the bulk eigenstates we have added an extra index to specify the type of material (well or barrier) the eigenfunction belongs to. The $\mathbf{g}_l$'s are the reciprocal-lattice vectors in the perpendicular direction associated with the mini-Brillouin-zone of the superlattice. They are given by

$$\mathbf{g}_l = (l-1)(2\pi/Ld)\hat{\mathbf{n}}, \quad l=1,2,\ldots,L \ . \tag{12}$$

Note that due to the periodicity of the superlayers in the superlattice, a superlattice eigenstate with the wave vector $\mathbf{k}_{\parallel}+\mathbf{q}$ has only contributions from the bulk eigenstates with wave vectors $\mathbf{k}_{\parallel}+(\mathbf{q}+\mathbf{g}_l)$, $l=1,2,\ldots,L$.

The envelope functions themselves are given by

$$F_n(\mathbf{k}_{\parallel}\mathbf{q},\mathbf{g}_l;j) = \frac{1}{\sqrt{L}} \sum_{\lambda\in j} \exp[-i(\mathbf{q}+\mathbf{g}_l)\cdot\lambda\mathbf{d}] C^n_{\lambda}(\mathbf{k}_{\parallel}\mathbf{q}), \quad j=W,B \ , \tag{13}$$

where the notation $\lambda \in j$ is used to specify whether λ is in the well or the barrier material. For instance, $\lambda \in W$ means that λ is in the well, i.e., $1 \le \lambda \le L_W$.

III. RESULTS AND DISCUSSION

In this section we examine the conduction bands of the (001) GaAs/$\mathrm{Al}_x\mathrm{Ga}_{1-x}\mathrm{As}$ and $\mathrm{Al}_x\mathrm{Ga}_{1-x}\mathrm{As}$/AlAs superlattices as obtained by the one-band Wannier orbital model. The AlGaAs superlattices are suitable candidates for treatment by the one-band Wannier orbital model. Both GaAs and AlAs are wide-gap semiconductors for which the conduction bands and valence bands can be treated separately. In addition, for both materials the second conduction band is sufficiently higher than the first so that the superlattice states of interest are derived almost completely from the lowest bulk conduction band. More precisely, in both GaAs and AlAs, the lowest point of the second conduction band is at the X point, and the separation between X_{3C} and X_{1C} for GaAs and AlAs are 0.4 eV (Ref. 17) and 0.2 eV (Ref. 18), respectively. Our one-band results are valid for energy range sufficiently below the X_{3C} point.

The one-band coefficients for GaAs, $\mathrm{Al}_{0.5}\mathrm{Ga}_{0.5}\mathrm{As}$, and AlAs are obtained by band-structure fitting, and are listed in the Appendix. Coefficients for other compositions of the $\mathrm{Al}_x\mathrm{Ga}_{1-x}\mathrm{As}$ alloy are obtained by quadratic interpolation. Using a quadratic rather than a linear interpolation scheme allows us to include the bowing of the band gaps.[19] In our calculations we use a conduction-band offset of $Q_e=0.7$,[10,11,20] meaning that 70% of the direct-band-gap difference between the well and the barrier materials is associated with the conduction band. Also, we choose the valence-band top of bulk GaAs to be zero in energy. We shall use the notation (L_W,L_B)-(001) $\mathrm{Al}_{x_W}\mathrm{Ga}_{1-x_W}\mathrm{As}/\mathrm{Al}_{x_B}\mathrm{Ga}_{1-x_B}\mathrm{As}$ to denote a superlattice with growth axis along the [001] direction, and with each period of the superlattice consisting of L_W layers of $\mathrm{Al}_{x_W}\mathrm{Ga}_{1-x_W}\mathrm{As}$ followed by L_B layers of $\mathrm{Al}_{x_B}\mathrm{Ga}_{1-x_B}\mathrm{As}$. Also, since for (001) superlattices $\mathbf{k}_{\parallel}$ has nonzero components only along the $\hat{\mathbf{x}}$ and $\hat{\mathbf{y}}$ directions, and $\mathbf{q}$ along the $\hat{\mathbf{z}}$ direction, for simplicity we will denote $\mathbf{k}_{\parallel}$ by the ordered pair (k_x,k_y), and $\mathbf{q}$ by the scalar q. For convenience, wave vectors will be given in units of $(2\pi/a)$, a being the lattice constant.

Before we present our results, we first make a few simple observations about the AlGaAs superlattices which will help us interpret our findings. Recall that we have designated the slabs with lower Al concentration as the well material and the slabs with higher Al concentration as the barrier material. With the $Q_e=0.7$ band offset, the X minima of the barrier material are always lower than those of the well material. The Γ minimum, on the other hand, is always lower in the well material. This means that in an AlGaAs superlattice, the electrons near the X minima see the slabs with higher Al concentration as the wells, while the electrons near the Γ minimum see the slabs with lower Al concentration as the wells. For convenience, we will call these the X wells and Γ wells, respectively. For example, in the $\mathrm{Al}_x\mathrm{Ga}_{1-x}\mathrm{As}$/AlAs superlattice, the AlAs layers are the X wells, and $\mathrm{Al}_x\mathrm{Ga}_{1-x}\mathrm{As}$ layers are the Γ wells. It should be noted that the Γ wells are always deeper than the X wells. However, depending on the compositions of the well and barrier materials, the bottom of the X well could be lower than the bottom of the Γ well.

An important factor in determining the superlattice band structure is the electron effective masses. (Recall from the simple particle-in-the-box model that the quantum-well energy levels are inversely proportional to the particle mass.) For the (001) superlattice, the three important effective masses are the Γ-valley effective mass (m_{Γ}), the X-valley longitudinal effective mass (m_l), and the X-valley transverse effective mass (m_t). They are, as obtained in our model, respectively, $0.067m_0$, $3.86m_0$, and $0.39m_0$ for GaAs, and $0.124m_0$, $1.82m_0$, and $0.23m_0$ for AlAs. The Γ mass of GaAs is in good agreement with the accepted experimental value.[21] The other values are less well established experimentally; our values are in general agreement with the various experimental values compiled by Madelung *et al.*[22] The important thing to remember here is that the longitudinal X mass is large, the transverse X mass is smaller, and the Γ mass is very small.

We now present our results, which are organized into three categories. In Sec. III A we study the dependence of the conduction bands on alloy composition, in Sec. III B we examine the effects of external hydrostatic pressure, and in Sec. III C we investigate the dependence on the wave vectors. In addition, dependence on layer thicknesses will also be explored as we go along.

A. Composition dependence

We examine the dependence of the conduction-band energy levels of the (001) GaAs/Al$_x$Ga$_{1-x}$As and Al$_x$Ga$_{1-x}$As/AlAs superlattices on the alloy composition x. Figures 2(a), 2(b), and 2(c) show the conduction-band energy levels of the zone-center states ($\mathbf{k}_\parallel = 0$, $q = 0$) of the (001) GaAs/Al$_x$Ga$_{1-x}$As superlattice as functions of alloy composition x for the following layer thicknesses: (a) $L_W = 7$, $L_B = 28$ [denoted by (7,28)]; (b) $L_W = 28$ [denoted by (28,28)]; (c) $L_W = 28$, $L_B = 7$ [denoted by (28,7)]. The superlattice energies are drawn with solid lines (——) for the even-parity states, and dashed lines (— — —) for the odd-parity states. Here parity is defined with respect to the center of the well material. On each graph the energies of the bulk Al$_x$Ga$_{1-x}$As alloy at Γ and X have been drawn in with dotted lines (· · · ·) for comparison. In this case the bulk Γ and X levels, respectively, indicate the top of the Γ well and bottom of the X well as functions of x. The bottom of the Γ well and the top of the X well are, respectively, fixed at 1.43 and 1.9 eV, as appropriate for room temperature. All results in this paper should be shifted up by 0.09 eV in order to compare with experimental data at zero temperature. The effect of increasing x, the Al mole fraction in the barrier material, is to (1) raise the top of the Γ well while keeping its bottom fixed, and (2) lower the bottom of the X well while keeping its top fixed. Knowing this makes it very simple to identify the Γ-well and the X-well states: The curves for the Γ-well states increase with x and are bounded above by the bulk Γ level, and the X-well states' curves decrease with x and are bounded below by the bulk X level. Unconfined states can also be seen on these graphs. Most of the states that lie above 1.9 eV (X-well top) are unconfined states.

In Fig. 2(b) where the thicknesses of the GaAs (Γ well) and Al$_x$Ga$_{1-x}$As (X well) slabs are equal, we see that the X-well states are spaced more closely together than the Γ-well states. This is due to the fact that the X well has a heavier quantization mass than the Γ well. In Fig. 2(c) the X-well width is decreased to seven layers ($\sim$20 Å), while the Γ-well width is kept at 28 layers. We see that while this has little effect on the confined Γ-well states, it substantially decreases the number of confined states in the X wells.

Next we compare Fig. 2(a) to Fig. 2(b). Going from Fig. 2(b) to 2(a) we decrease the Γ-well width to seven layers. Decreasing the well width squeezes the Γ-well confined states up in energy so that for $x > 0.63$, the lowest conduction-band state is an X-well state, in spite

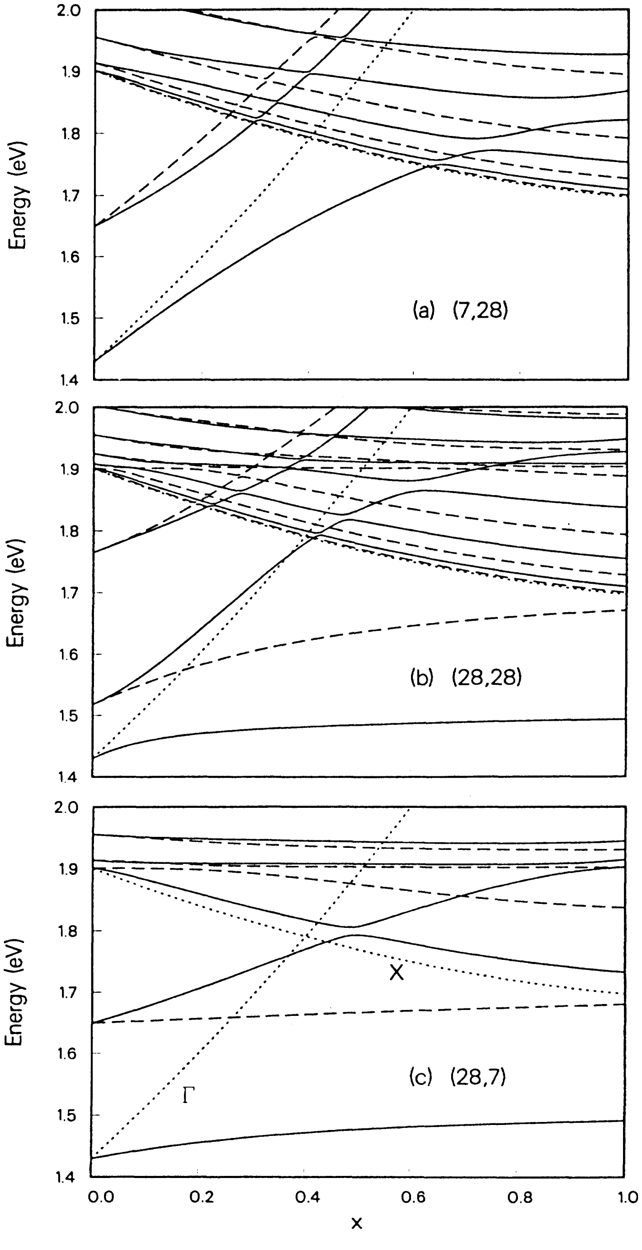

FIG. 2. Conduction-band energy levels of the $\mathbf{k}_\parallel = 0$, $q = 0$ states of the (001) GaAs/Al$_x$Ga$_{1-x}$As superlattice as functions of alloy composition x. Layer thicknesses are as follows: (a) (7,28), (b) (28,28), and (c) (28,7). The superlattice energies are drawn with solid lines (——) for the even-parity states and dashed lines (— — —) for the odd-parity states. The energies of the bulk Al$_x$Ga$_{1-x}$As alloy at Γ and X are drawn in with dotted lines (· · · ·) for comparison.

of the fact that the bottom of the Γ well is about 300 meV lower than the bottom of the X well. Note that the Γ-well states are much more sensitive to the change in well width than the X-well states. By comparing Fig. 2(c) to 2(b), we see that for the GaAs/AlAs superlattice, decreasing the X-well width from 80 to 20 Å raises the lowest X-well state by about 40 meV. Comparing Fig. 2(a) to 2(b), we see that the same change in the Γ-well width raises the lowest Γ-well state by about 300 meV. This is due to the fact that the Γ effective mass is much lighter than the longitudinal X mass, which in this case is the quantization mass for the X wells. Recall from the simple particle-in-the-box model that the energy levels are inversely proportional to the product of the particle mass and the square of the well width. Therefore the changes in energy levels due to changes in well width are amplified by a factor inversely proportional to the effective mass.

We now turn to the case where the barrier material is fixed as AlAs while the composition of the well material $\mathrm{Al}_x\mathrm{Ga}_{1-x}\mathrm{As}$ is varied. Figures 3(a), 3(b), and 3(c) show the conduction-band energy levels of the zone-center states ($\mathbf{k}_{\parallel}=0$, $q=0$) of the (001) $\mathrm{Al}_x\mathrm{Ga}_{1-x}\mathrm{As}$/AlAs superlattice as functions of alloy composition x for the following layer thicknesses: (a) $L_W=7$, $L_B=28$; (b) $L_W=28$, $L_B=28$; (c) $L_W=28$, $L_B=7$. The legends used in this figure are the same as in Fig. 2. In this case, the top of the Γ well is fixed at 2.48 eV while the bottom of the Γ well increases with x, as indicated by the dotted line corresponding to the bulk Γ level. The bottom of the X well is fixed at 1.69 eV while the top decreases as a function of x, as indicated by the bulk X level. So, again, the curves for the Γ-well states increase with x and are bounded below by the bulk Γ level, and the X-well states' curves decrease with x and are bounded above by the bulk X level.

The dependence of the energy levels on the layer thicknesses is again evident as we compare the three graphs in Fig. 3. In Figs. 3(b) and 3(c), the lowest conduction-band state changes from a Γ-well state to an X-well state as we increase x. For Fig. 3(a), however, the Γ well is so thin that the lowest state is always an X-well state. An $\mathrm{Al}_x\mathrm{Ga}_{1-x}\mathrm{As}$/AlAs superlattice in which the lowest conduction-band state is an X-well state is considered a type-II superlattice; that with a Γ-well state being the lowest conduction-band state is considered type I.

Whether an $\mathrm{Al}_x\mathrm{Ga}_{1-x}\mathrm{As}$/AlAs superlattice is type I or type II depends on the layer thicknesses and the alloy composition. Typically, as in Figs. 3(b) and 3(c), when we increase x from 0, the superlattice changes from type I to type II at some composition x_C. We call x_C the "crossover composition." Note that we can immediately conclude that x_C must be less than 0.4, since for $x>0.4$ the Γ-well bottom is higher than the X-well top, so the lowest state must be an X-well state.

In Fig. 4 the crossover composition of the (001) $\mathrm{Al}_x\mathrm{Ga}_{1-x}\mathrm{As}$/AlAs superlattice is plotted as a function of the well width L_W for several fixed values of L_B. Note that by decreasing the Γ-well width L_W we can substantially lower the crossover composition. In fact, as we have seen in Fig. 3(c), for L_W sufficiently small, the superlattice is always type II, regardless of the alloy composition. Note also that x_C decreases as the X-well width L_B is increased. This is because widening the X well lowers the X-well states, making them easier for the Γ-well states to overtake. The dependence of x_C on the X-well width, however, is not as strong as the depen-

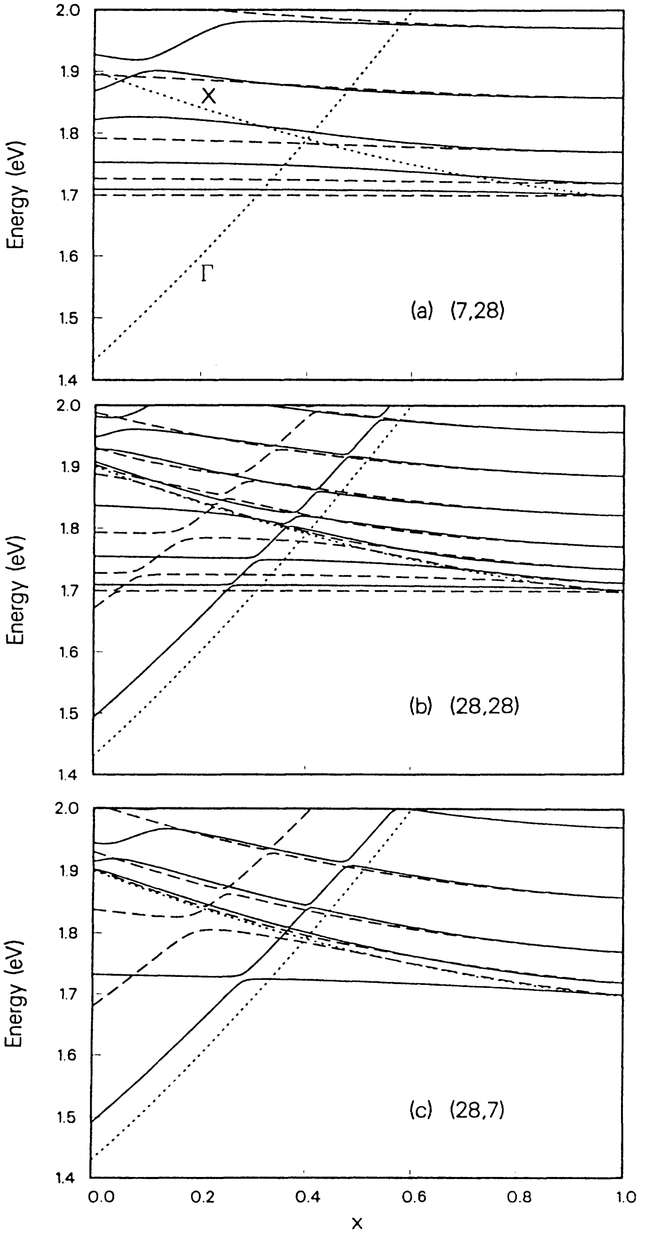

FIG. 3. Conduction-band energy levels of the $\mathbf{k}_{\parallel}=0$, $q=0$ states of the (001) $\mathrm{Al}_x\mathrm{Ga}_{1-x}\mathrm{As}$/AlAs superlattice as functions of alloy composition x. Layer thicknesses are as follows: (a) (7,28), (b) (28,28), and (c) (28,7). The superlattice energies are drawn with solid lines (——) for the even-parity states and dashed lines (— — —) for the odd-parity states. The energies of the bulk $\mathrm{Al}_x\mathrm{Ga}_{1-x}\mathrm{As}$ alloy at Γ and X are drawn in with dotted lines (· · · ·) for comparison.

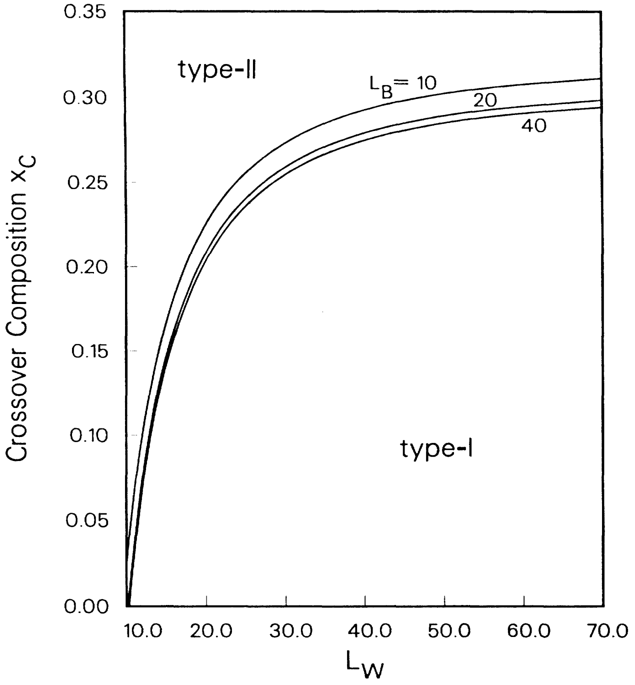

FIG. 4. Crossover composition of the (001) Al$_x$Ga$_{1-x}$As/AlAs superlattice as a function of the well width L_W for several fixed values of L_B.

dence on the Γ-well width.

We now take a closer look at the nature of the crossovers. In Fig. 5 we have plotted the energy levels of the $\mathbf{k}_{\parallel}=0$, $q=0$ states of the (001) Al$_x$Ga$_{1-x}$As/AlAs superlattice as functions of x near the crossover point. The layer thicknesses are (28,8) for Fig. 5(a), and (28,7) for Fig. 5(b). Note that in Fig. 5(a), the crossover composition x_C is well defined. In Fig. 5(b) however, the curves for the lowest X-well state and the lowest Γ-well state anticross, leaving no clearly defined crossover point. Upon closer examination we note when an X-well state curve meets a Γ-well state curve; they cross if they have different parities and anticross if they have the same parity. This is since the quantum well has even parity, so that an X-well state and a Γ-well state close in energy can interact with each other only if they have the same parity. The interaction gives rise to the anticrossing behavior. What is puzzling is this: In going from Fig. 5(a) to 5(b), the only change we have made is to reduce the thickness of the AlAs layers from eight to seven. But notice the dramatic change: While the Γ-well states remain essentially the same, all the X-well states have switched parity. For instance, the lowest X-well state in the (28,7) superlattice has even parity, but the lowest X-well state in the (28,8) superlattice has odd parity. The parity switch of the X-well states in turn changes all the crossings to anticrossings and vice versa. To understand this we need to look at the wave functions.

In Fig. 6 we've plotted the coordinate space envelope functions of the lowest two states for each of the two superlattices at the crossover composition $x_C=0.28$. In

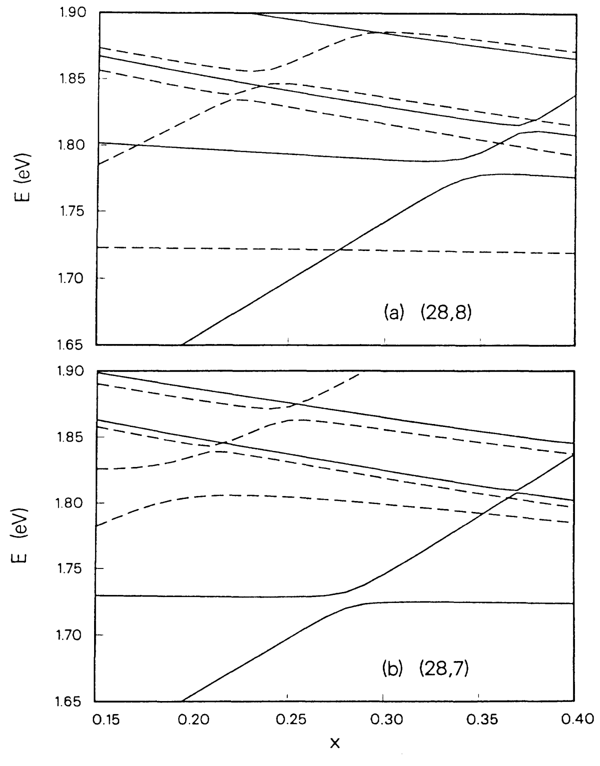

FIG. 5. Energy levels of the (001) Al$_x$Ga$_{1-x}$As/AlAs superlattice as functions of x near the crossover point. The layer thicknesses are (28,8) in (a), and (28,7) in (b).

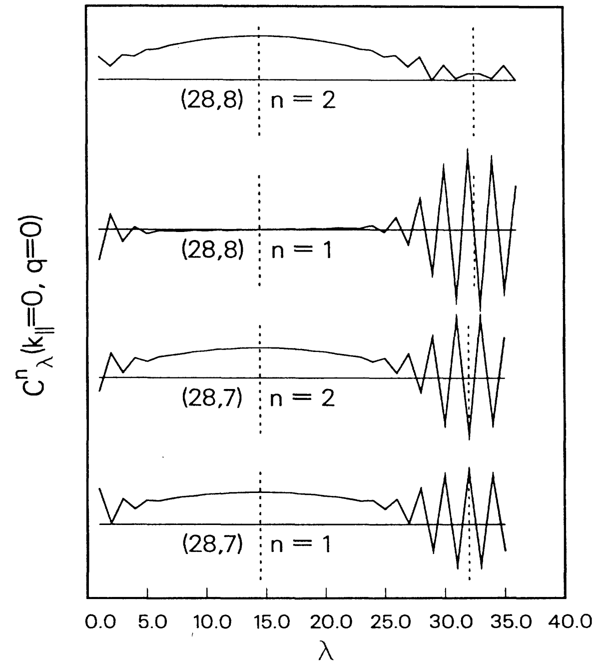

FIG. 6. Coordinate space envelope functions of the lowest two $\mathbf{k}_{\parallel}=0$, $q=0$ states for the (28,8)- and (28,7)-(001) Al$_{0.28}$Ga$_{0.72}$As/AlAs superlattices.

these graphs $1 \leq \lambda \leq 28$ corresponds to the $Al_{0.28}Ga_{0.72}As$ layers, with the remaining corresponding to the AlAs layers. The well and barrier centers are indicated by vertical dotted lines. Note that at $q=0$, the superlattice wave function is invariant under a translation of distance Ld along the z direction; hence the parities of the states with respect to the well center and the barrier center are the same. We first look at the (28,8) case where the lowest Γ-well and X-well states do not interact. The $n=2$ state is the lowest Γ-well state and its envelope function is just the typical particle-in-the-box ground-state wave function. The $n=1$ state is the lowest X-well state. In general, the X-well state wave functions can be described by the particle-in-the-box wave functions modulated by a phase factor $\exp(i\mathbf{X}\cdot\mathbf{R})$, since the X-well state comes from electrons near the $\mathbf{X}=(0,0,1)(2\pi/a)$ point in the Brillouin zone. For the lowest-lying X-well state, the particle-in-the-box wave function is even with respect to the barrier center, and the parity of the state is determined by the phase factor. We write the phase factor as $\cos(2\pi R_z/a)+i\sin(2\pi R_z/a)$, where R_z is the z component of $\mathbf{R}$ measured from the barrier center. When the X well consists of an even number of layers, R_z must take on values like $(m+\frac{1}{2})(a/2)$, where m is an integer; thus the cosine term in the phase factor vanishes and the wave function is odd with respect to the barrier center. This explains why the lowest X-well state in the (28,8) superlattice is an odd parity state. When the X well consists of an odd number of layers, R_z must take on values like $m(a/2)$; thus the sine term vanishes and the wave function is even.

For the (28,7) superlattice, the lowest X-well and Γ-well states have the same parity; they interact when they are brought close together in energy at the crossover composition. The Γ-X mixing results in the mixture states that we see in the bottom two graphs of Fig. 6.

Since we are looking at the superlattice envelope functions, we should point out another interesting phenomenon. The superlattice states we have examined so far all have $q=0$. Recall that the superlattice envelope functions carry a q-dependent phase factor $\exp(iSL\mathbf{q}\cdot\mathbf{d})$, which is a constant within a superlayer but changes from one superlayer to the next. In general, because of this modulating phase factor, the superlattice envelope functions do not have definite parities, except when $q=0$, where the phase factor is always 1. There is another q for which we can associate parities with the superlattice envelope functions, and that is $q=(\pi/Ld)\equiv q_{\max}$. At $q_{\max}$, the phase factor becomes $(-1)^S$, alternatingly assuming the values of 1 and -1 going from one superlayer to the next. This forces the envelope functions to have the opposite parities with respect to the well and barrier centers. This is demonstrated in Fig. 7, where we have plotted envelope functions for the same superlattices as in Fig. 6, except here we have $q=q_{\max}$ instead of $q=0$. As we can see, each of the $q=q_{\max}$ states is at once both even and odd, depending on whether parity is defined with respect to the center of the Γ well or the X well.

An interesting consequence of all this is that the Γ-X crossing and anticrossing rule for the $q=q_{\max}$ case is the opposite of the $q=0$ case. At $q=0$, when the curves for the lowest Γ-well and X-well states meet, they cross if L_B is even, and anticross if L_B is odd. For $q=q_{\max}$, the opposite is true. This can be seen by comparing Figs. 6 and 7. For $L_B=8$, the lowest Γ-well and X-well states are decoupled at $q=0$, but mixed at $q=q_{\max}$. The opposite is true for $L_B=7$.

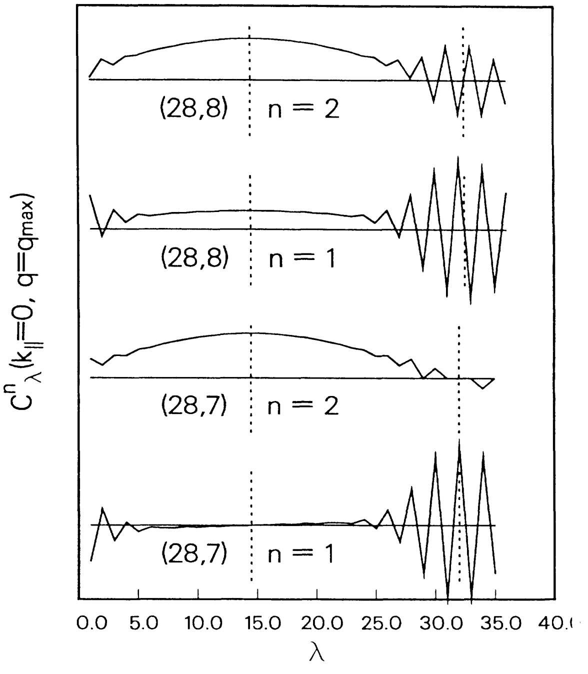

FIG. 7. Coordinate space envelope functions of the lowest two $\mathbf{k}_\parallel=0$, $q=q_{\max}$ states for the (28,8)-, and (28,7)-(001) $Al_{0.28}Ga_{0.72}As$/AlAs superlattices.

B. Pressure dependence

In this section we study the effects of hydrostatic pressure on the superlattice conduction bands. In general, applying hydrostatic pressure to bulk $Al_xGa_{1-x}As$ moves the Γ valley up and X valley down. In addition, the Γ-valley effective mass also increases with pressure. We know this from the $\mathbf{k}\cdot\mathbf{p}$ theory which tells us that the Γ-valley effective masses increase as the direct band gap widens. In the $\mathbf{k}\cdot\mathbf{p}$ theory, we have $m_0/m_\Gamma=1+C/E_g(P)$, where C is a constant proportional to the squared momentum matrix element between the conduction- and valence-band states.[23] In our model the pressure-induced changes of the Γ-valley effective mass and the Γ-, X-, and L-valley positions are incorporated by modifying the one-band coefficients.

In Fig. 8 we plotted the energy levels of $\mathbf{k}_\parallel\mathbf{q}=0$ states for the (25,50)-(001) $GaAs/Al_{0.3}Ga_{0.7}As$ superlattice as functions of applied hydrostatic pressure. For GaAs, the Γ-, X-, and L-valley pressure coefficients we used are, respectively, 10.7, -1.3, and 2.8 (in units of meV/kbar).[10,24] For AlAs, the corresponding pressure coefficients are 9.9, -0.9, and 2.8.[10,24] As we can see

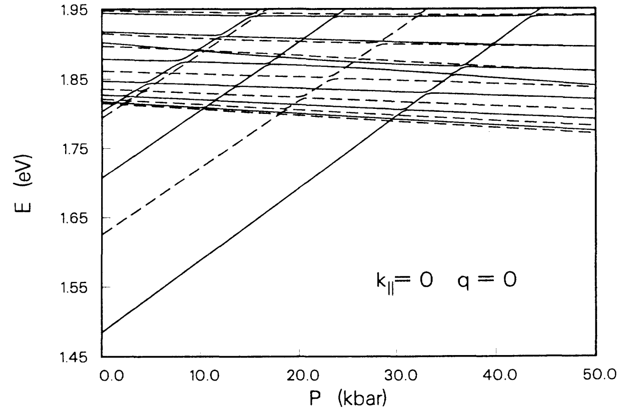

FIG. 8. Energy levels of zone center states for the (25,50)-(001) GaAs/Al$_{0.3}$Ga$_{0.7}$As superlattice as functions of applied hydrostatic pressure.

from the numbers, the effect of hydrostatic pressure is to move the Γ well up and the X well down, accompanied by some small changes in the well depths. The effects are analogues to the changes caused by varying the alloy compositions which we discussed in Sec. III A. We can identify the curves for Γ-like states by their positive slopes, and the X-like states by their negative slopes. Note that at $P\approx 29$ kbar the lowest Γ-like state overtakes the lowest X-like state, indicating a type-I to type-II transition. The pressure where this type-I to type-II transition occurs is called the "crossover pressure."

In Fig. 9 we plot the crossover pressures for the (001) GaAs/Al$_{0.3}$Ga$_{0.7}$As superlattices as functions of well width L_W for several fixed values of L_B. The features in this figure are similar to those found in Fig. 4 where we plotted the crossover composition. As in Fig. 4, by decreasing the Γ-well width L_W we can lower the crossover point. The explanation is similar and we will not repeat it here. We should mention that for bulk GaAs, the Γ-X crossover occurs at $P\approx 40$ kbar. The superlattice crossover pressures are lower.

In Fig. 10 we plot the pressure coefficients α_Γ for the lowest few Γ-well states in (001) GaAs/Al$_{0.3}$Ga$_{0.7}$As superlattices. The width of the barrier slabs is taken to be sufficiently large so that the GaAs slabs can be considered as isolated quantum wells. The superlattice α_Γ's are obtained by computing the rates of increase of the Γ-well energy levels with pressure. The E versus P curves actually deviate from being strictly linear, but we will ignore the small nonlinearity here. The solid curves in Fig. 10 represent results obtained with our one-band model. The dashed curves are obtained by using a particle-in-the-box model in which the particle mass is allowed to vary with pressure; and the top and the bottom of the quantum well vary with pressure according to the bulk Al$_{0.3}$Ga$_{0.7}$As and GaAs α_Γ's, respectively. The

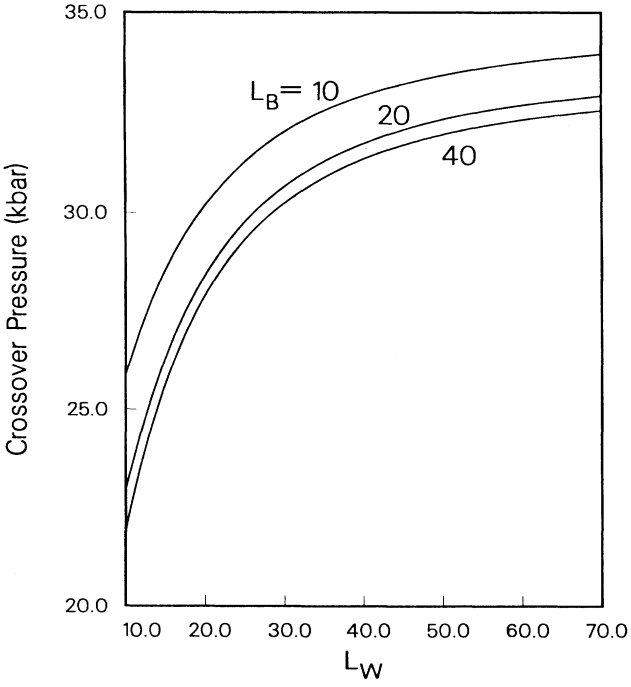

FIG. 9. Crossover pressures for (001) GaAs/Al$_{0.3}$Ga$_{0.7}$As superlattices as functions of well width L_W for several fixed values of L_B.

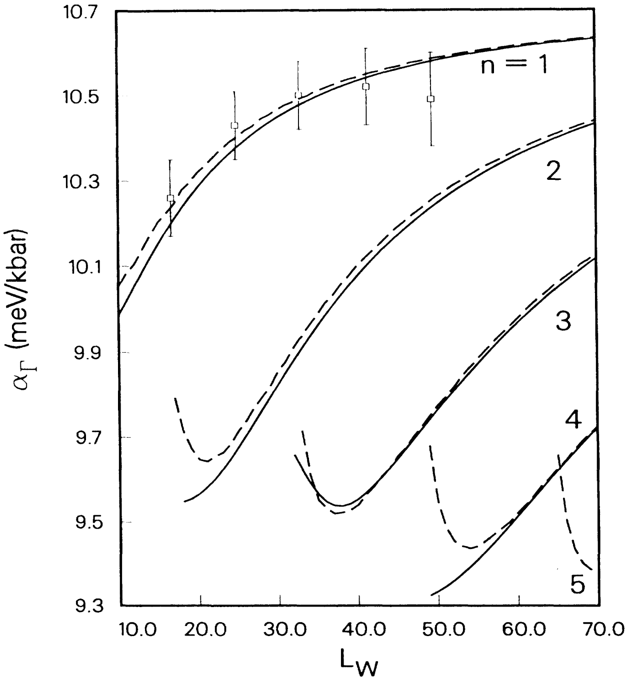

FIG. 10. Pressure coefficients α_Γ for the lowest few confined Γ-well states in (001) GaAs/Al$_{0.3}$Ga$_{0.7}$As superlattices as functions of well width L_W. The solid curves represent results obtained with the one-band model. The dashed curves are obtained by using a particle-in-the-box model in which the particle mass is allowed to vary with pressure; the top and the bottom of the well vary with pressure according to the bulk Al$_{0.3}$Ga$_{0.7}$As and GaAs α_Γ's, respectively. The open squares represent the experimental values for the $n=1$ quantum-well state obtained by Venkateswaran *et al.* (Ref. 10).

open squares represent the experimental values for the $n=1$ quantum-well state obtained by Venkateswaran *et al.*[10] Our theoretical values are in good agreement with the experimental results. We note first of all that while α_Γ for bulk GaAs is 10.7 meV/kbar, the superlattice α_Γ's are noticeably smaller. At first we might suspect that this is due to the leakage of the superlattice wave functions into the $\mathrm{Al_{0.3}Ga_{0.7}As}$ slabs in which the pressure coefficient is smaller (9.9 meV/kbar). A simple calculation will show that this effect is too small to account for the difference between the bulk GaAs and the superlattice α_Γ's. The real explanation is due to the fact that the Γ-valley effective mass increases with pressure. This in turn causes the Γ-well energy levels relative to the Γ-well bottom to decrease with pressure. This means that the rates of increase for the Γ-well levels with respect to pressure is smaller than that for the bulk Γ valley, resulting in α_Γ's that are smaller than the bulk value.

A general feature of the α_Γ curves is that they decrease with increasing n, and, except for the "hooks" at the end of the curves, decrease with decreasing L_W. To explain this we recall that for the particle-in-the-box problem the energy levels relative to the well bottom are approximately given by (assuming large barrier height):

$$E_n \approx \frac{\pi^2\hbar^2 n^2}{2mL_W^2} \; . \tag{14}$$

We see that the decrease in E_n due to the pressure-induced increase in effective mass is amplified by factors of n^2 and $1/L_W^2$. Since decrease in E_n causes the quantum-well α_Γ's to be reduced from the bulk value, we expect this reduction to increase with n and decrease with L_W. Note that one of the effects of the finite barrier height is the "hooks" that we see. The hooks are associated with quantum-well levels near the well top which cannot be approximated by (14).

Recall from our discussion in Sec. III A that when the E versus x curves belonging to Γ-well states and X-well states meet, they either cross or anticross, depending on whether there is Γ-X mixing. Recall also that the crossing or anticrossing behavior depends critically on the thickness of the X well, and that changing the X-well thickness by one monolayer would reverse the crossing or anticrossing patterns completely. Here we shall suggest a way by which this dependence of crossing or anticrossing patterns on whether the X well consists of an even or an odd number of monolayers might be observed with pressure experiments.

Consider an experiment in which we are trying to observe the luminescence associated with transitions from the lowest conduction subband to the highest valence subband as functions of pressure. When pressure is increased, the lowest conduction-subband states cross over from Γ-like to X-like, while the highest valence subband states remain Γ-like. Since the overlap between the conduction-band X-like state and the valence-band Γ-like state is small, we would expect the luminescence intensity to drop off as we increase the pressure past the crossover point. How quickly the intensity drops off depends on whether we have a "crossing" or an "anticrossing."

The difference between Γ-X crossing and anticrossing is illustrated in Fig. 11 where we have plotted the square of the k-space envelope function $[\,|F_n(\mathbf{k}_\parallel q, \mathbf{g}_l; j)|^2$, $j=W,B]$ of the lowest conduction-band state at $\mathbf{k}_\parallel=0$, $q=0$ for the (7,7)- and the (8,8)-(001) GaAs/$\mathrm{Al_{0.3}Ga_{0.7}As}$ at several different pressures near the crossover point. In the (7,7) (anticrossing) case, the wave function gradually changes from being Γ-like (consisting mainly of components from near $k_z=0$) to X-like (consisting mainly of components from near $k_z=1$), with intermediate states being Γ-X mixed states. In the (8,8) (crossing) case, the Γ-X crossover is abrupt, with no Γ-X mixing. From this we would expect the luminescence intensity as a function of pressure to drop off gradually for the anticrossing case, and abruptly for the crossing case.

However, the story is not quite this simple. Recall that for a given superlattice subband the crossing and anticrossing patterns are the opposite for $q=0$ and $q=q_{\max}$. Typically we would not be able to isolate these crossing and anticrossing patterns from each other if the subbands associated with the states of interest have small dispersion in the $\hat{\mathbf{z}}$ direction, so that the states with different q's in the lowest subband would all be occupied, giving us a q-averaged luminescence. However, in the case when the well and barrier thicknesses are ultrathin, the lowest subband can actually have considerable dispersion as a function of q. This is illustrated in Fig. 12 where we have plotted the q dispersion curves for the (7,7)- and the (28,28)-(001) GaAs/$\mathrm{Al_{0.3}Ga_{0.7}As}$ at $\mathbf{k}_\parallel=0$. As we can see, whereas the lowest subband for the (28,28) case is virtually dispersionless, the energy difference between the $q=0$ and $q=q_{\max}$ states for the lowest subband for the (7,7) case is around 250 meV. This means that in the ultrathin case, we only need to consider the states near $q=0$ for luminescence.

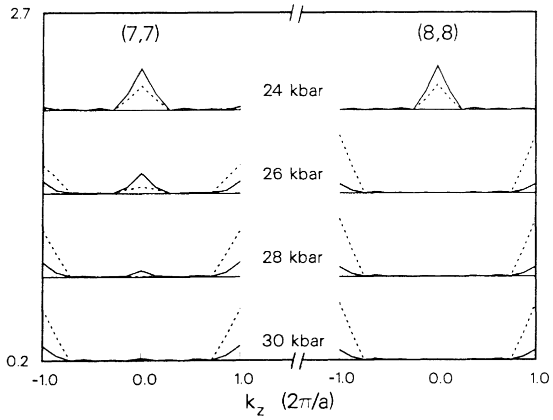

FIG. 11. Square of the k-space envelope function $(\,|F_n(\mathbf{k}_\parallel q, \mathbf{g}_l; j)^2$, $j=W,B)$ of the lowest conduction-band state at $\mathbf{k}_\parallel=0$, $q=0$ for the (7,7)- and the (8,8)-(001) GaAs/$\mathrm{Al_{0.3}Ga_{0.7}As}$ at several different pressures near the crossover point. The $j=W$ (well component) is represented by the solid curve, and the $j=B$ (barrier component) is represented by the dotted curve.

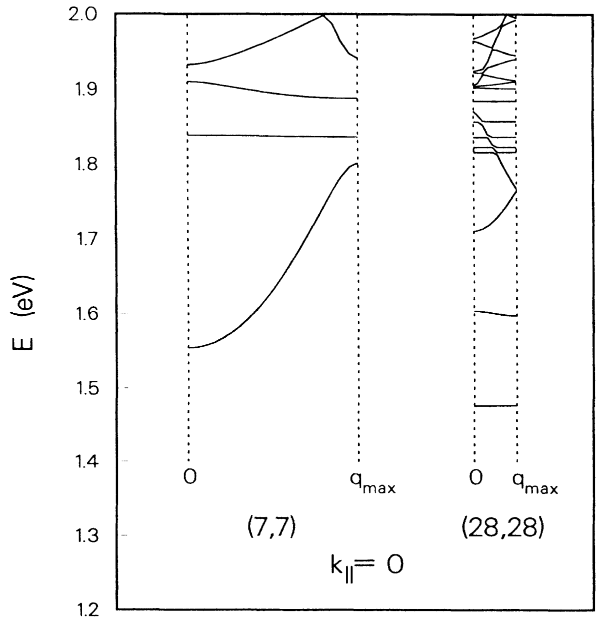

FIG. 12. q dispersion curves for the (7,7)- and the (28,28)-(001) GaAs/Al$_{0.3}$Ga$_{0.7}$As at $\mathbf{k}_{\|}=0$.

Figure 13 shows the luminescence for the (7,7) and the (8,8) superlattices as a function of pressure. The luminescence is simulated by calculating the square of the overlap of the envelope functions for the $\mathbf{k}_{\|}=0$, $q=0$ states of the lowest conduction subband and the highest valence subband. In the (7,7) case, we have Γ-X mixing and the luminescence drops off gradually. For the (8,8) case, the Γ and X states do not mix, and the luminescence drops off sharply. In fact, it drops off to zero since the lowest $q=0$ X-well state for the (8,8) case is odd. This is one way by which the crossing or anticrossing dependence on the X-well thickness might be observed. Note that in order to observe this we must have samples in which the superlattice well and barrier thicknesses are ultrathin, and precise to one monolayer.

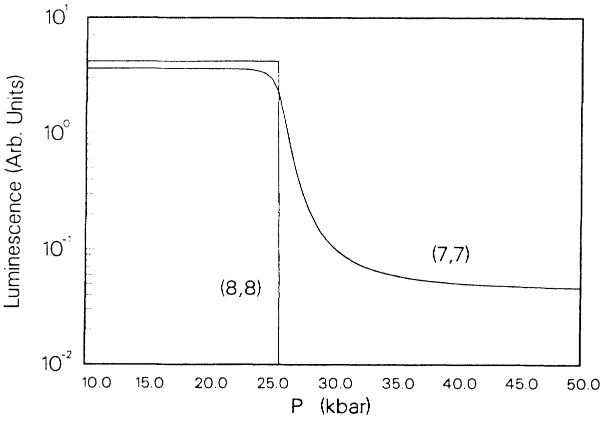

FIG. 13. Simulated luminescence for the (7,7)- and the (8,8)-(001) GaAs/Al$_{0.3}$Ga$_{0.7}$As superlattices as a function of pressure.

C. Dependence on $k_{\|}$

So far, we have only looked at states at $\mathbf{k}_{\|}=\mathbf{0}$. In this section we examine the dependence of the superlattice energy levels on $\mathbf{k}_{\|}$. In Fig. 14 we plot the energy levels of the (28,28)-(001) Al$_{0.25}$Ga$_{0.75}$As/AlAs superlattice as functions of k_x, with k_y and q fixed at 0. Again, the solid and dashed curves are used to identify the even- and odd-parity states, respectively. The parity is for reflection about a plane parallel to the interface and through the well center. The interesting feature of Fig. 14 is that, as a result of zone folding, it contains information about quantum-well states associated with all three of the X valleys as well as the Γ valley. To distinguish the (100), (010), and (001) X valleys we shall refer to them as, respectively, the X_x, X_y, and the X_z valley. Note that here X valleys and Γ valley refer to the X valleys of AlAs and the Γ valley of AlGaAs.

To illustrate how the various X valleys come into play, in Fig. 15 we plotted the lowest conduction band of bulk AlAs along the direction of zone folding ($\hat{\mathbf{z}}$) for fixed values of k_x and k_y. The solid curve ranges from $\mathbf{k}=(1,0,-1)$ to (1,0,1), and describes the bulk states that are folded into the $\mathbf{k}_{\|}=(1,0)$ superlattice states which appear on the right-hand side of Fig. 14. This includes the (100) (X_x) and the (010) X-valley (X_y) states. [Note: the (010) point is equivalent to the (101) point in k space because they differ by a reciprocal-lattice vector $(1\bar{1}1)$.] It is interesting to note that the band structure is symmetric with respect to the line $k_z=0.5(2\pi/a)$. The dotted curve ranges from $\mathbf{k}=(0,0,-1)$ to (0,0,1), and describes the bulk states that are folded into the $\mathbf{k}_{\|}=(0,0)$ superlattice states which appear on the left-hand side of Fig. 14. This includes the X_z-valley states.

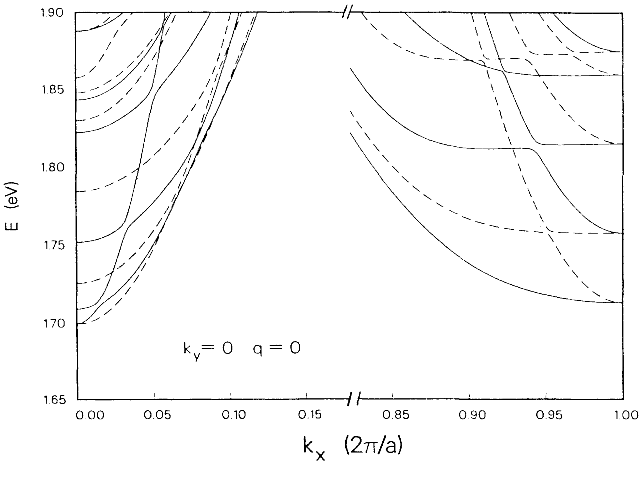

FIG. 14. Energy levels of the (28,28)-(001) Al$_{0.25}$Ga$_{0.75}$As/AlAs superlattice as functions of k_x, with k_y and q fixed at 0. The solid and dashed curves are used to identify the even- and odd-parity states, respectively.

TABLE I. Effective masses of the Γ and X valleys.

	[100] mass (dispersion mass)	[001] mass (quantization mass)
X_x (100)	m_l	m_t
X_y (010)	m_t	m_t
X_z (001)	m_t	m_l
Γ (000)	m_Γ	m_Γ

Note from Fig. 15 that the [001] effective mass is different for the three X valleys. For the X_z valley, it is the (heavier) longitudinal mass m_l, and for the X_x and X_y valleys, it is the (lighter) transverse mass m_t. The mass along [001] is important because it is the quantization mass in the (001) superlattices. The other important quantity here is the [100] effective mass. The [100] mass accounts for the dispersion along [100], the direction along which the band structure is being examined in Fig. 14. The types of effective masses associated with the Γ and the X valleys are summarized in Table I.

We are now able to identify the various subbands in Fig. 14. First of all, we know that the X_z-valley states are folded into the region around $\mathbf{k}_\parallel=(0,0)$ along with the Γ-valley states. If we look at the left-hand side of Fig. 14, we can see that there are two subbands associated with the Γ valley (starting at about 1.7 and 1.86 eV). The Γ subbands are marked by their larger curvature due to the smaller Γ-valley dispersion mass. The other subbands are associated with the X_z valley.

Turning to the right-hand side of Fig. 14 (near $K_x=1$), we again see two sets of curves. As we have discussed earlier, both the X_x- and X_y-valley states are folded into the region near $\mathbf{k}_\parallel=(1,0)$. From Table I we see that X_x-valley states have a larger dispersion mass than the X_y valley. We can therefore identify the set of curves with the smaller curvature as the X_x-valley states, and the other set as the X_y-valley states.

We note that all the X_x- and X_y-valley states at $\mathbf{k}_\parallel=(1,0)$ come in degenerate pairs. The X_x- and X_y-valley states are in the same quantum well (the X well), and they have the same quantization mass, so we might expect them to be degenerate. However, the degeneracy is not necessary. In Fig. 16 we plotted the band structure along k_x again, keeping the circumstances the same as in Fig. 14, except changing the layer thicknesses from (28,28) to (27,27). Note that this time the degeneracy at $\mathbf{k}_\parallel=(1,0)$ is lifted. Comparing this band structure with that in Fig. 14, we note that they are almost identical, except that the parities of all the X_y-valley states have been reversed. The dependence of parity on layer thicknesses reminds us of the Γ-X crossover in Fig. 5. And in fact, the explanations in both cases are the same. Once again, the envelope functions for the $\mathbf{k}_\parallel=(1,0)$ states associated with the X_x valley are essentially the particle-in-the-box wave functions as in the case of the Γ-valley states, while those associated with the X_y valley [(101) X valley] are particle-in-the-box wave functions modulated by a phase factor. When the modulating phase factor is an odd function (L_B even), the X_x and X_y states have different parities, and they do not interact. But when the modulating phase factor is an even function (L_B odd), the X_x and X_y states have the same parity and interact with each other to lift the degeneracy. We shall call this interaction "X_x-X_y mixing," in analogy to

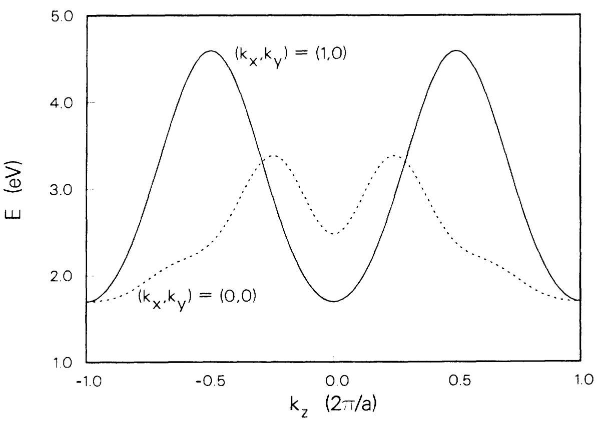

FIG. 15. Lowest conduction band of bulk AlAs along the direction of zone folding ($\hat{z}$) for fixed values of k_x and k_y. The solid curve corresponds to $(k_x,k_y)=(1,0)$, and the dotted curve corresponds to $(k_x,k_y)=(0,0)$.

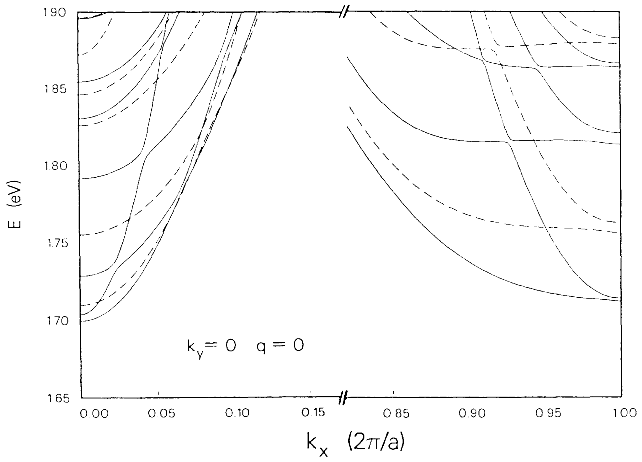

FIG. 16. Energy levels of the (27,27)-(001) $Al_{0.25}Ga_{0.75}As/AlAs$ superlattice as functions of k_x, with k_y and q fixed at 0. The solid and dashed curves are used to identify the even- and odd-parity states, respectively.

Γ-X mixing (hereafter referred to as the Γ-X_z mixing to avoid confusion with the X_x and X_y states). We point out that both X_x-X_y mixing and Γ-X_z mixing can be seen in Fig. 16. We have chosen the alloy compositions such that we are at a Γ-X_z crossover point. In Fig. 14, the lowest Γ-well state and the lowest X-well states at $\mathbf{k}_{\parallel}=(0,0)$ are (accidentally) degenerate. In Fig. 16, the degeneracy is lifted, giving us Γ-X_z mixing states at $\mathbf{k}_{\parallel}=(0,0)$.

Another feature that can be seen in Figs. 14 and 16 is the role of quantization mass. By comparing the energy levels of the lowest X-well states at $\mathbf{k}_{\parallel}=(0,0)$ and $\mathbf{k}_{\parallel}=(1,0)$, which we abbreviate as $X^{(0,0)}$ and $X^{(1,0)}$, we see that $X^{(0,0)}$ is always lower in energy. This is because $X^{(0,0)}$ is associated with the X_z valley, which has a larger (001) quantization mass than the X_x or the X_y valley. To illustrate this further, in Fig. 17 we plotted the energy levels of $X^{(0,0)}$ and $X^{(1,0)}$ for the (N,N)-(001) Al$_{0.25}$Ga$_{0.75}$As/AlAs superlattice as functions of layer thicknesses N. For comparison $\Gamma^{(0,0)}$, the lowest Γ state, is also included. We keep the Γ-well and X-well widths the same ($L_W=L_B=N$) so we can make reasonable comparisons between the Γ-well and X-well states. Solid circles are used to indicate an odd-parity state, open circles for an even-parity state, and solid squares for a degenerate pair of even and odd states. Note that, due to its larger quantization mass, $X^{(0,0)}$ is always lower than $X^{(1,0)}$, which is either an X_x-X_y mixed state (L_B odd) as in Fig. 16, or an X_x,X_y twofold-degenerate state (L_B even) as in Fig. 14. $\Gamma^{(0,0)}$, as we have mentioned before in Figs. 2 and 3, is lower than the X states at large N, but is higher than the X states for small N. Note that there are some wiggles in the Γ curve at small N where $\Gamma^{(0,0)}$ is higher than $X^{(0,0)}$. This is due to the interaction between the lowest Γ-well state and some higher X-well states. The wiggles in the $X^{(1,0)}$ curve are due to the fact that the X_x-X_y mixing occurs only if L_B is odd. As we can see, X_x-X_y mixing is more pronounced at smaller values of N.

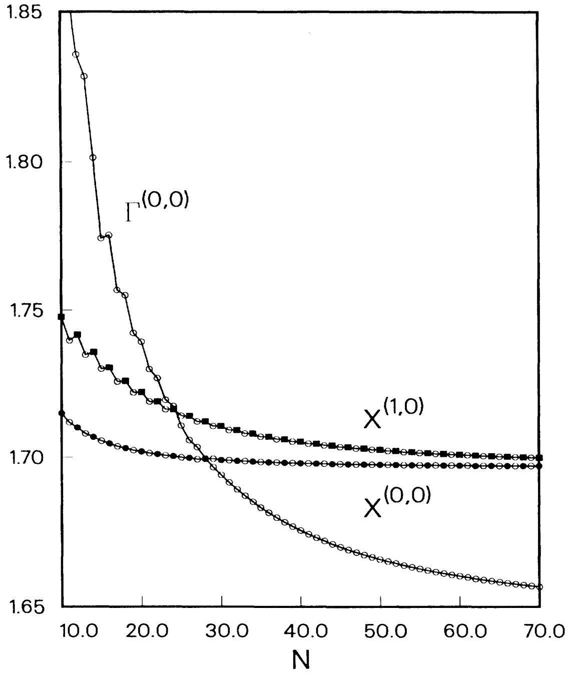

FIG. 17. Energy levels of the lowest Γ-well state ($\Gamma^{(0,0)}$), the lowest X-well state at $\mathbf{k}_{\parallel}=(0,0)$ ($X^{(0,0)}$), and the lowest X-well state at $\mathbf{k}_{\parallel}=(1,0)$ ($X^{(1,0)}$) for the (N,N)-(001) Al$_{0.25}$Ga$_{0.75}$As/AlAs superlattice as functions of layer thickness N. A solid circle is used to denote an odd-parity state, an open circle denotes an even-parity state, and a solid square denotes a degenerate pair of even and odd states.

IV. SUMMARY

We have developed an efficient and realistic model for studying the conduction bands of superlattices made from indirect-band-gap semiconductors. Using this model we have made a systematic study of the conduction bands of the (001) GaAs/Al$_x$Ga$_{1-x}$As and Al$_x$Ga$_{1-x}$As/AlAs superlattices.

In treating this problem we found that it is convenient to think of the superlattice as consisting of different types of quantum wells: Γ well for the Γ-valley electrons and X well for the X-valley electrons. In the Al$_x$Ga$_{1-x}$As superlattices, the Γ wells and the X wells are staggered, with the Γ well in the slabs with lower Al concentration and the X well in the slabs with higher Al concentration.

A primary objective of ours is to study the confined states associated with the indirect valleys which are folded into the reduced Brillouin zone. In the case of the (001) Al$_x$Ga$_{1-x}$As superlattices, for instance, we have the X_z valley which is folded into $\mathbf{k}_{\parallel}=(0,0)$, and the X_y valley which is folded into $\mathbf{k}_{\parallel}=(1,0)$. The envelope functions of these confined states can be considered as particle-in-the-box wave functions modulated by a spatially varying phase factor. This phase factor has an important effect on the property of the envelope function. At $q=0$, for example, the modulating phase factor associated with the X_z and the X_y valleys is either an even- or an odd-paritied function, depending on whether the width of the X well, L_B, is an odd or an even number, respectively. Therefore, in this case the overall parity of the envelope functions is dependent on the thickness of the X well.

The phase factor is important because it can determine how the confined states interact with one another. By appropriately adjusting the alloy compositions or external hydrostatic pressure, we can bring the confined states associated with the different conduction-band valleys close together in energy to see how they interact with each other. In our case, the Γ-valley states and the X_z-valley states can be brought together at $\mathbf{k}_{\parallel}=(0,0)$, and so can the X_x and the X_y valleys at $\mathbf{k}_{\parallel}=(1,0)$. We find that Γ-X_z mixing and X_x-X_y mixing are similar in nature. The only difference is that the (100) and the (010) X valleys have the same quantization mass, while the Γ valley and the (001) X valley have different quantization masses. At $q=0$, states from different valleys can mix only if they have the same parity. Since the parity of the zone-folded states is determined by the X-well layer thickness, we find that Γ-X_z and X_x-X_y mixing is dependent on the X-well thickness. In addition, we also found that Γ-X_z and X_x-X_y mixing also depend on the superlattice wave vector q. For instance, if for a particular superlattice Γ-X_z mixing occurs at $q=0$, then the Γ state and the X state are noninteracting at $q=q_{\max}$.

In studying the pressure dependence of the (001) GaAs/$\mathrm{Al}_x\mathrm{Ga}_{1-x}$As superlattice, we found that the pressure coefficient of the superlattice states associated with the Γ valley are all smaller than the bulk α_Γ. The amount that they deviate from the bulk α_Γ depends on the well width L_W and the principal quantum number n. In general, the deviation decreases with L_W and increases with n. This is explained in terms of the dependence of the Γ-valley effective mass on the applied hydrostatic pressure. The theoretical results obtained with our model are found to be in good agreement with experimental values.

One of our findings is that both Γ-X_z mixing and X_x-X_y mixing are enhanced when the layer thicknesses are small. Our calculation also shows that pressure experiment on high quality samples of superlattices with ultrathin layers can offer us a way to observe the dependence of Γ-X_z mixing on the X-well width.

In conclusion we would like to remark that we have found the one-band Wannier orbital model to be invaluable in our studies of the properties of $\mathrm{Al}_x\mathrm{Ga}_{1-x}$As superlattices. Its numerical efficiency allows us to generate data on different aspects of the problem quickly, and its simplicity makes interpreting the data easy. We believe this method can be a valuable tool in studying other types of superlattices as well.

Note added. We would like to direct the readers' attention to a paper by Jaros and co-workers[25] which appeared after our manuscript was submitted. In that article the electronic and optical properties of the GaAs/$\mathrm{Al}_x\mathrm{Ga}_{1-x}$As superlattice as functions of alloy composition and hydrostatic pressure are studied using the pseudopotential method. The results that they presented are in general qualitative agreement with ours.

ACKNOWLEDGMENTS

The authors have benefited from fruitful discussions with M. Chandrasekhar. This work was supported by the U.S. Office of Naval Research (ONR) under Contract No. N00014-81-K-0430. The use of the computing facilities of the University of Illinois Materials Research Laboratory under a National Science Foundation (NSF) grant is gratefully acknowledged.

APPENDIX

In this appendix we discuss the details of how the one-band parameters are obtained, and how they are modified phenomenologically to account for the effects of hydrostatic pressure.

1. Fitting one-band parameters

We first derive an expression for $E(\mathbf{k})$ which we use in fitting the one-band parameters. The bulk band structure in the one-band Wannier orbital model is related to the matrix elements between Wannier orbitals as follows:

$$E(\mathbf{k})=\sum_{\mathbf{R}}\exp(i\mathbf{k}\cdot\mathbf{R})\langle \mathbf{O}\,|\,H\,|\,\mathbf{R}\rangle \ , \tag{A1}$$

where $\mathbf{R}$ specifies the coordinates of the unit cell in which the Wannier orbital $|\,\mathbf{R}\rangle$ is located, and $\mathbf{O}$ is the origin. For convenience, in the remainder of this section we shall write R in units of $a/4$, and $\mathbf{k}$ in units of $2\pi/a$, where a is the lattice constant. In these units, $\mathbf{R}$ is given by a triplet of integers (l,m,n).

We define a "shell" as a collection of all lattice points located at equivalent positions relative to the origin [e.g., $\mathbf{R}=(2,2,0)$ and $\mathbf{R}'=(0,-2,2)$ are on the same shell]. We label the shells by the index i, and specify the ith shell by the triplet (l_i,m_i,n_i), the coordinates of a lattice point on the ith shell. In our calculations 21 shells are used. A listing of (l_i,m_i,n_i) is given in Table II. Note that even though (6,6,0) and (8,2,2) are equidistant from the origin, they are considered to be on two separate shells.

Due to the symmetry of the Wannier orbitals, if $\mathbf{R}$ and $\mathbf{R}'$ are on the same shell, then $\langle \mathbf{O}\,|\,H\,|\,\mathbf{R}\rangle=\langle \mathbf{O}\,|\,H\,|\,\mathbf{R}'\rangle$. We can therefore use a single number C_i to denote the matrix element $\langle \mathbf{O}\,|\,H\,|\,\mathbf{R}^{(i)}\rangle$, where $\mathbf{R}^{(i)}$ could be any lattice point on the ith shell. For convenience, we refer to the C_i's as the one-band parameters. By grouping the terms involving $\mathbf{R}$'s on the same shell together in Eq. (A1), we can write $E(\mathbf{k})$ as

$$E(\mathbf{k})=\sum_i C_i S_i(l_i,m_i,n_i;\mathbf{k}) \ , \tag{A2}$$

where summation index i runs over the shells, and S_i is the "shell structure factor" associated with the ith shell:

$$S_i(l_i,m_i,n_i;\mathbf{k})=\sum_{\mathbf{R}\in i\text{th shell}}\exp(i\mathbf{k}\cdot\mathbf{R}) \ . \tag{A3}$$

It can be shown that S_i is given by

$$S_i(l,m,n;\mathbf{k})=\frac{N_i}{6}\sum_{P}F(\mathbf{P}(l),\mathbf{P}(m),\mathbf{P}(n);\mathbf{k}) \ , \tag{A4}$$

where N_i is the number of points in the ith shell, and the sum is taken over all permutations $(\mathbf{P})$ of (l,m,n). F is given by

$$F(l,m,n;\mathbf{k})=\cos\left(lk_1\frac{\pi}{2}\right)\cos\left(mk_2\frac{\pi}{2}\right)\cos\left(nk_3\frac{\pi}{2}\right) \ . \tag{A5}$$

Equation (A2) is used in our band-structure fitting procedure. In fitting the band structure, one of the most critical quantities is the Γ-valley effective mass m_Γ. It can be shown that the Γ-valley effective mass is given by

$$\left(\frac{m_0}{m_\Gamma}\right)=-\frac{1}{96\mathrm{Ry}}\left(\frac{a_0}{a}\right)^2\sum_i C_iN_i(l_i^2+m_i^2+n_i^2) \ , \tag{A6}$$

where Ry is the Rydberg constant, m_0 is the free-electron mass, and a_0 is the Bohr radius.

TABLE II. Al$_x$Ga$_{1-x}$As one-band coefficients for $x=0$, 0.5, and 1. Coefficients for other compositions are obtained from values given here by quadratic interpolation. The onsite energy (C_1) listed in this table are adjusted to give $E(\mathbf{k}=0)=0$. For use in superlattices, the offset of $1.425+Q_e(1.155x+0.37x^2)$ eV should be added to the onsite values.[17]

Shell index i	$\mathbf{R}$ $\left[\frac{a}{4}\right]$	R^2 $\left[\left[\frac{a}{4}\right]^2\right]$	N_i	$C_i(\langle \mathbf{O}\mid H\mid \mathbf{R}\rangle)$ (eV) GaAs	Al$_{0.5}$Ga$_{0.5}$As	AlAs
1	(0,0,0)	0	1	3.0864	3.2219	3.4322
2	(2,2,0)	8	12	−0.0297	−0.0033	0.0309
3	(4,0,0)	16	6	0.0064	−0.0467	−0.0989
4	(4,2,2)	24	24	0.0492	0.0206	−0.0163
5	(4,4,0)	32	12	−0.1212	−0.1099	−0.1065
6	(6,2,0)	40	24	0.0012	0.0105	0.0256
7	(4,4,4)	48	8	−0.0216	−0.0137	0.0015
8	(6,4,2)	56	48	0.0110	0.0269	0.0483
9	(8,0,0)	64	6	0.0819	0.0060	−0.0775
10	(6,6,0)	72	12	−0.0528	−0.0741	−0.0946
11	(8,2,2)	72	24	−0.0252	0.0014	0.0356
12	(8,4,0)	80	24	0.0053	0.0279	0.0497
13	(6,6,4)	88	24	0.0079	−0.0014	−0.0175
14	(8,4,4)	96	24	0.0041	0.0027	0.0032
15	(8,6,2)	104	48	0.0041	−0.0136	−0.0376
16	(10,2,0)	104	24	−0.0016	−0.0203	−0.0478
17	(10,4,2)	120	48	−0.0029	0.0030	0.0094
18	(8,8,0)	128	12	−0.0388	−0.0154	0.0112
19	(8,6,6)	136	24	−0.0199	−0.0013	0.0191
20	(10,6,0)	136	24	−0.0094	0.0007	0.0173
21	(8,8,4)	144	24	0.0014	−0.0124	−0.0259

The band-structure fitting procedure is as follows: First, $E(\mathbf{k})$ at 60 point along the path $L-\Gamma-X-U-L-W-K-\Gamma-W-X$ in the Brillouin zone is computed by using the pseudopotential method. Where necessary, the $E(\mathbf{k})$'s are adjusted slightly to give better agreement with known experimental values. A search in the parameter space $\{C_i\}$ is then conducted to find the set of one-band parameters which, when used in Eq. (A2), yields the band structure which most closely approximates the adjusted pseudopotential band structure. In the fitting process, more weight is given to the points with lower energies since the superlattice states of interest come mainly from bulk states in this energy range. Also, heavy emphasis is placed on obtaining a good fit to the Γ-valley effective mass.

The one-band parameters for GaAs and AlAs are listed in Table II. The pseudopotential form factors for GaAs and AlAs used in band-structure fitting are taken from Caruthers and Lin-Chung.[26]

2. Pressure effects

In treating the effects of hydrostatic pressure we try to account for the changes in the energies of the Γ, X, and L valleys and the change in the Γ-valley effective mass by modifying the values of the one-band parameters. The pressure-induced changes in energy at the Γ, X, and L points are given by

$$E_\Gamma(P)=E_\Gamma(0)+\alpha_\Gamma P\ , \tag{A7a}$$

$$E_X(P)=E_X(0)+\alpha_X P\ , \tag{A7b}$$

$$E_L(P)=E_L(0)+\alpha_L P\ , \tag{A7c}$$

where P is the pressure, and the α's are the bulk pressure coefficients associated with the three conduction-band valleys. Note that we have assumed that the valence-band tops of the well and the barrier materials do not move relative to each other as a function of pressure. In other words, the pressure changes in the band gaps have been completely assigned to the conduction band. This assumption is in good agreement with recent first-principles calculations by Van de Walle and Martin[27] which showed that in AlGaAs heterostructures the pressure-induced change in the difference of the valence-band tops (ΔE_v) is more than an order of magnitude smaller than the change in the band-gap difference (ΔE_g).

The change in the Γ-valley effective mass, as described in Sec. III B, is given by

$$\frac{m_0}{m_\Gamma(P)}=1+\frac{C}{E_\Gamma(P)}\ . \tag{A8}$$

The procedure we use to modify the one-band parameters to account for these changes involves two steps. First we scale all the parameters by the pressure dependent factor $f(P)$:

$$C_i' = f(P) C_i \ , \tag{A9a}$$

$$f(P) = \frac{m_\Gamma(P=0)}{m_\Gamma(P)} \ . \tag{A9b}$$

As we can easily verify by using Eq. (A6), the scale parameters $\{C_i'\}$ give us a band structure with the desired $m_\Gamma(P)$. In fact, as we can see from Eq. (A2), the entire band structure is now scaled by a factor of $f(P)$.

We next try to simulate the changes in Γ, X, and L. We note that by scaling the one-band parameters we have modified the energies of Γ, X, and L. These changes must be compensated for in addition to the pressure-induced changes. Therefore, we now need to modify the scaled one-band parameters to affect the following changes in the Γ, X, and L energies:

$$\Delta\Gamma = \alpha_\Gamma P + [1 - f(P)] E_\Gamma(P=0) \ , \tag{A10a}$$

$$\Delta X = \alpha_X P + [1 - f(P)] E_X(P=0) \ , \tag{A10b}$$

$$\Delta L = \alpha_L P + [1 - f(P)] E_L(P=0) \ . \tag{A10c}$$

In addition, we have to ensure that whatever new changes we now make in the one-band parameters do not disturb the already correct $m_\Gamma(P)$. This is done by modifying the scaled parameters associated with the four smallest shells (C_1', C_2', C_3', C_4'). It can be shown that the proper changes that need to be made are

$$\Delta C_1' = (6\,\Delta\Gamma + 18\,\Delta X + 24\,\Delta L)/49 \ , \tag{A11a}$$

$$\Delta C_2' = (5\,\Delta\Gamma - 3\,\Delta X - 2\,\Delta L)/49 \ , \tag{A11b}$$

$$\Delta C_3' = (1\,\Delta\Gamma + 3\,\Delta X - 4\,\Delta L)/49 \ , \tag{A11c}$$

$$\Delta C_4' = (-1\,\Delta\Gamma + 1\,\Delta L)/49 \ . \tag{A11d}$$

We mention that the reason we did not simulate the changes in the Γ, X, and L energies and m_Γ by modifying the one-band parameters associated with the four smallest shells alone is that it would give us grossly distorted band structure in the rest of the Brillouin zone even at moderate pressures. The procedure that we used avoids this problem.

---

[1] L. Esaki and R. Tsu, IBM J. Res. Dev. **14**, 61 (1970).

[2] L. L. Chang and L. Esaki, in *Progress in Crystal Growth and Characterization,* edited by B. R. Pamplin (Pergamon, Oxford, 1979).

[3] R. Dingle, *Festkorperprobleme,* edited by J. Trensch (Pergamon, New York, 1975), Vol. 15, p. 21.

[4] Y.-C. Chang and J. N. Schulman, Appl. Phys. Lett. **43**, 536 (1983); Phys. Rev. B **31**, 2069 (1985).

[5] M. Altarelli, Phys. Rev. B **32**, 5138 (1985).

[6] G. D. Sanders and Y. C. Chang, Phys. Rev. B **31**, 6892 (1985); **35**, 1300 (1987).

[7] G. C. Osbourn, J. Vac. Sci. Technol. **21**, 469 (1982).

[8] P. L. Gourley and R. M. Biefeld, J. Vac. Sci. Technol. **21**, 473 (1982).

[9] J. C. Bean, T. T. Sheng, L. C. Feldman, A. T. Fiory, and R. T. Lynch, Appl. Phys. Lett. **44**, 102 (1984).

[10] U. Venkateswaran, M. Chandrasekhar, H. R. Chandrasekhar, B. A. Vojak, F. A. Chambers, and J. M. Meese, Phys. Rev. B **33**, 8416 (1986); Proceedings of the Second International Conference on Superlattices, Microstructures and Microdevices, Goteborg, Sweden, 1986 (unpublished).

[11] D. J. Wolford, T. F. Keuch, J. A. Bradley, M. A. Gell, D. Ninno, and M. Jaros, J. Vac. Sci. Technol. B **4**, 1043 (1986).

[12] B. A. Wilson, P. Dawson, C. W. Tu, and R. C. Miller, J. Vac. Sci. Technol. B **4**, 1037 (1986).

[13] E. Finkman, M. D. Sturge, and M. C. Tamargo, Appl. Phys. Lett. **49**, 1299 (1986).

[14] I. Morrison, M. Jaros, and K. B. Wong, J. Phys. C **19**, L239 (1986).

[15] M. A. Gell, D. Ninno, M. Jaros, and D. C. Herbert, Phys. Rev. B **34**, 2416 (1986).

[16] D. Z.-Y. Ting and Y.-C. Chang, J. Vac. Sci. Technol. B **4**, 1002 (1986).

[17] W. P. Dumke, M. R. Lorenz, and G. D. Pettit, Phys. Rev. B **5**, 2978 (1972).

[18] T. C. Chiang, J. A. Knapp, M. Anono, and D. E. Eastman, Phys. Rev. B **21**, 3515 (1980).

[19] H. J. Lee, L. Y. Juravel, J. C. Woolley, and A. J. Spring Thorpe, Phys. Rev. B **21**, 659 (1980).

[20] J. Menéndez, A. Pinczuk, A. C. Gossard, J. H. English, D. J. Werder, and M. G. Lamont, J. Vac. Sci. Technol. B **4**, 1041 (1986).

[21] H. C. Casey, Jr. and M. B. Panish, *Heterostructure Lasers* (Academic, New York, 1978), Pt. A.

[22] *Landolt-Börnstein: Numerical Data and Functional Relationships in Science and Technology,* edited by O. Madelung, M. Schulz, and H. Weiss, Group 3, Vol. 17(a) (Springer-Verlag, Berlin, 1982).

[23] See, for example, W. A. Harrison, *Solid State Theory* (McGraw-Hill, New York, 1970), p. 141.

[24] M. Chandrasekhar (private communication). The pressure coefficient is determined by a linear fit to the photoluminescence at 80 K as a function of pressure for pressures between 0 and 40 kbar.

[25] M. A. Gell, D. Ninno, M. Jaros, D. J. Wolford, T. F. Keuch, and J. A. Bradley, Phys. Rev. B **35**, 1196 (1987).

[26] Ed Caruthers and P. J. Lin-Chung, Phys. Rev. B **17**, 2705 (1978).

[27] C. G. Van de Walle and R. M. Martin, Phys. Rev. B **35**, 8154 (1987).